NANO LETTERS
Cite This: Nano Lett. XXXX, XXX, XXX−XXX
Letter
pubs.acs.org/NanoLett

Microcavity-Mediated Spectrally Tunable Amplification of Absorption in Plasmonic Nanoantennas

Qinglan Huang[†,‡] and Brian T. Cunningham*[,†,‡,§]

[†]Department of Electrical and Computer Engineering, [‡]Micro and Nanotechnology Laboratory, and [§]Department of Bioengineering, University of Illinois at Urbana−Champaign, Urbana, Illinois 61801, United States

Supporting Information

ABSTRACT: Nanoantenna−microcavity hybrid systems offer unique platforms for the study and manipulation of light at the nanoscale, since their constituents have either low mode volume or long photon storage time. A nearby dielectric optical cavity can modify the photonic environment surrounding a plasmonic nanoantenna, presenting opportunities to sculpt its spectral response. However, matching the polar opposites for enhanced light−matter interactions remains challenging, as the antenna can be rendered transparent by the cavity through destructive Fano interferences. In this work, we tackle this issue by offering a new plasmonic−photonic interaction framework. By coupling to a photonic crystal guided resonance, a gold nanostar delivers 1 order of magnitude amplified absorption, and the ultrasharp Lorentzian-line-shaped hybrid resonance is continuously tunable over a broad spectral range by scanning of the incidence angle. Our intuitive coupled mode model reveals that a distinct optical pathway highlighting the cavity-mediated activation of nanoantennas is key for absorption enhancement. Moreover, we show that the line width of the enhancement can be widely tunable, and that the maximum power transferred to the antennas is attained under critical coupling. The cooperative hybrid system opens up new opportunities to boost a wealth of applications including ultrasensitive molecular spectroscopy, plasmonic hot carrier chemistry, thermoplasmonic, spontaneous emission enhancement, nanolasers, and many more.

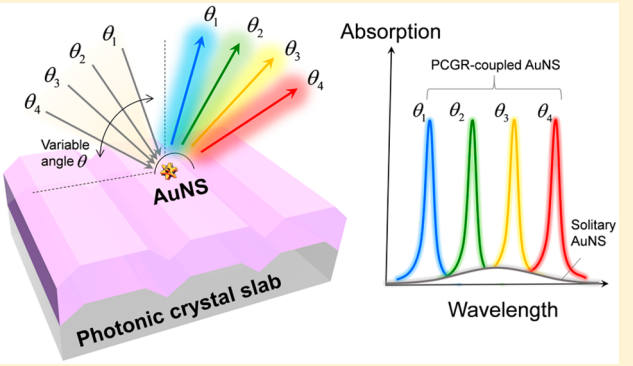

KEYWORDS: *Optical microcavity, photonic crystal, plasmonic nanoantenna, coupling, absorption enhancement*

Plasmonic nanoantennas are key elements in the conversion of radiative waves into intense, nanoscale localized fields,[1] enabling strong light−matter interactions that underpin a wealth of applications including plasmon-induced hot carrier technology,[2] thermoplasmonics,[3] spontaneous emission enhancement,[4] surface-enhanced spectroscopy,[5,6] nanolasers,[7] nonlinear optics,[8] and quantum plasmonics.[9] Optical absorption induced in the plasmonic nanoantenna, a local quantity calculated by integrating the product of frequency, local electric field intensity, and the imaginary part of the dielectric permittivity over the volume of the nanoantenna, is of particular interest as it characterizes the strength of its interplay with light.[10] The enhancement of absorption, signifying amplification of optical field localized at the plasmonic resonator, is limited by rapid plasmon dephasing through radiative and nonradiative channels.[11] It is intuitive to interface a plasmonic nanoantenna with a dielectric optical microcavity (for instance, a Fabry−Perot cavity,[12,13] a whispering-gallery-mode (WGM) cavity,[14] or a photonic crystal[15]) which features an extended photon lifetime[16] to attain stronger light−matter interactions. Recently, we reported enormous near-field enhancement when gold nanorods are coupled to an on-resonant (that is, $\omega_a = \omega_c$) photonic crystal guided resonance (PCGR).[17] Despite a few successful examples, however, it remains unclear how to coordinate the two polar opposites to synergistically combine an antenna's mode confinement and a cavity's optical feedback. Typically, the plasmonic−photonic hybridization undergoes Fano interference with a strikingly different phenomenon: an on-resonant optical cavity effectively depolarizes the plasmonic antenna in analogous to electromagnetically induced transparency (EIT),[18] diminishing its absorption over a narrow spectral window,[19−21] and absorption enhancement is often only bestowed with an antenna−cavity resonance frequency detuning, where asymmetric Fano line shapes occur.[15,22−25] Why does an on-resonant microcavity enhance the near field of the antenna in one case, but suppress it in another case? Under what conditions would a microcavity *always* cooperate with a nanoantenna regardless of their frequency detuning?

This letter addresses these questions by studying a broadly representative plasmonic−photonic hybrid resonator system comprised of gold nanostars (AuNSs) deposited on a photonic

Received: April 30, 2019
Revised: July 11, 2019
Published: July 17, 2019

DOI: 10.1021/acs.nanolett.9b01764
Nano Lett. XXXX, XXX, XXX−XXX

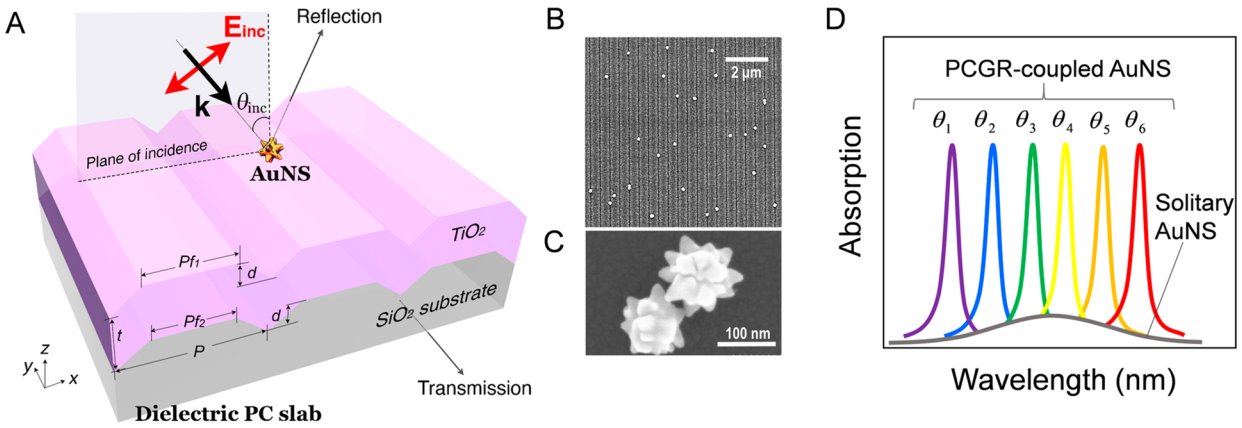

Figure 1. AuNS–PCGR hybrid structure for spectrally tunable absorption enhancement. (A) Schematic illustration of the hybrid system consisting of individual gold nanostars (AuNSs) dispersed on the surface of a dielectric photonic crystal (PC) slab (TiO_2 coated on the AuNS is omitted). TM-polarized light (incident electric field lying in the plane of incidence) excites the plasmonic–photonic hybrid resonance at incident angle θ_{inc}, and the zeroth-order transmittance and reflectance are measured to probe the AuNSs' extinction. Structure parameters of the PC slab: P = 460 nm, f_1 = 0.6, f_2 = 0.55, t = 187 nm, d = 80 nm. The geometry of the AuNS is described in the Supporting Information. Scanning electron microscopy images of the (B) hybrid structure and (C) AuNSs. (D) Compared to solitary AuNSs, PCGR-coupled ones deliver significantly enhanced absorption. The ultrasharp hybrid resonance is spectrally tunable with broad-band coverage by continuous scanning of the incidence angle.

crystal (PC) slab. Far-field measurements of the AuNS–PCGR hybrid under different polarizations and incidence angles demonstrate that the cavity mediates a strong absorption enhancement of 1 order of magnitude, and the sharp resonance is spectrally tunable from visible to near-infrared ranges. Here the moderate-Q PCGR microcavity serves as a low-loss storage of the optical field, while the optical antenna AuNS creates nanometer-scale hotspots, leading to vigorous optical energy extraction at the nanoscale. With an intuitive temporal coupled mode theory (TCMT)[26,27] model, we attribute the absorption enhancement to unique optical pathways (in contrast to typical Fano interactions where the "bright" antenna mode is driven directly by external fields and subject to backaction of the "dark" cavity mode, here the narrowband cavity resonance channels energy between the external fields and the broadband antenna resonance). We show that a judicious coordination of the PCGR's Q-factor and surface density of the antennas is critical to achieve maximum absorption. Our result can be generalized to interface broad classes of resonant nanophotonic building blocks, offering a new perspective on enhancing light–matter interactions. The efficient energy coupling to the nanoscale is ideal for ultrasensitive molecular spectroscopy, artificial photosynthesis, nonlinear optics, creating nanoscopic heat sources, and many more.

The AuNS–PCGR hybrid system is composed of individual AuNSs (acting as plasmonic nanoantennas) located on the surface of a PC slab (acting as a dielectric microcavity) (Figure 1A). Their spectral and spatial modal overlap gives rise to near-field coupling of the plasmonic and photonic resonances, forming a hybrid supermode that combines the cavity's high Q-factor and antenna's small mode volume. The PC slab is comprised of a TiO_2 (n = 2.3) film deposited on a quartz (n = 1.47) substrate that is periodically modulated along the x-direction. When meeting the phase-matching conditions, a transverse magnetic (TM) polarized plane wave (with the incident electric field component lying in the x–z plane) excites twin counterpropagating leaky modes in the corrugated TiO_2 film.[28,29] Continuous scanning of the incidence angle produces ultrasharp PCGRs (Q = 400 at λ = 795 nm) with broad spectral coverage from 600 to 1000 nm. The open-face architecture of the PC slab lends itself well to large-area fabrication and enables simple integration with plasmonic antennas in various forms, including colloidal metal nanoparticles, lithographically patterned nanostructures, synthesized antenna–reactor composites, and movable metallic tips.[30] Here, we choose the spiky AuNSs (diameter 100 nm, Figure 1C) as an example because (1) compared to nanorods, their symmetric structure enables efficient antenna–cavity coupling that is insensitive to the orientation of the nanoparticle, and (2) compared to nanospheres, their sharp tips accommodate multiple strong electromagnetic hotspots.[31] The very low surface density (Figure 1B) of the AuNSs excludes interparticle coupling. As we shall see later, the AuNS density has an impact on the resonant absorption strength and line width. To compensate for the wavelength mismatch between the pristine AuNSs and the PCGRs, a thin film of TiO_2 was deposited onto the hybrid structure to red shift the plasmon resonance[32] to λ = 795 nm, such that the tunable PCGRs are encompassed inside (Figure S2).

One unique feature of our antenna–cavity hybrid system is that the cavity effect can be disentangled *in situ*, as PCGRs can be switched on/off through changing the polarization or incidence angle of the excitation beam, allowing a direct comparison between the solitary and cavity-coupled antennas. We interrogate the extinction of the same antennas under different coupling scenarios through probing the specular reflectance R and zeroth-order transmittance T spectra of the composite (Figure 1A). The low-loss bare PCGR mode is associated with a sharp peak (dip) in the R (T) spectrum, with R+T approaching 1 (Figure S1; a small discrepancy comes from scattering due to surface roughness). Upon coupling to lossy plasmonic nanoparticles, a prominent drop (rise) in the resonant reflection peak (transmission dip) intensity occurs, accompanied by broadening of the resonance line width, signaling the formation of a plasmonic–photonic supermode (Figure S3). By energy conservation, these spectral characteristics stem from energy extinction in the nanoparticles, specifically, 1-R-T = Abs + S, where Abs and S are the absorption and nonzeroth order scattering of the antennas, respectively.[33] While it is hard to distinguish between

DOI: 10.1021/acs.nanolett.9b01764
Nano Lett. XXXX, XXX, XXX–XXX

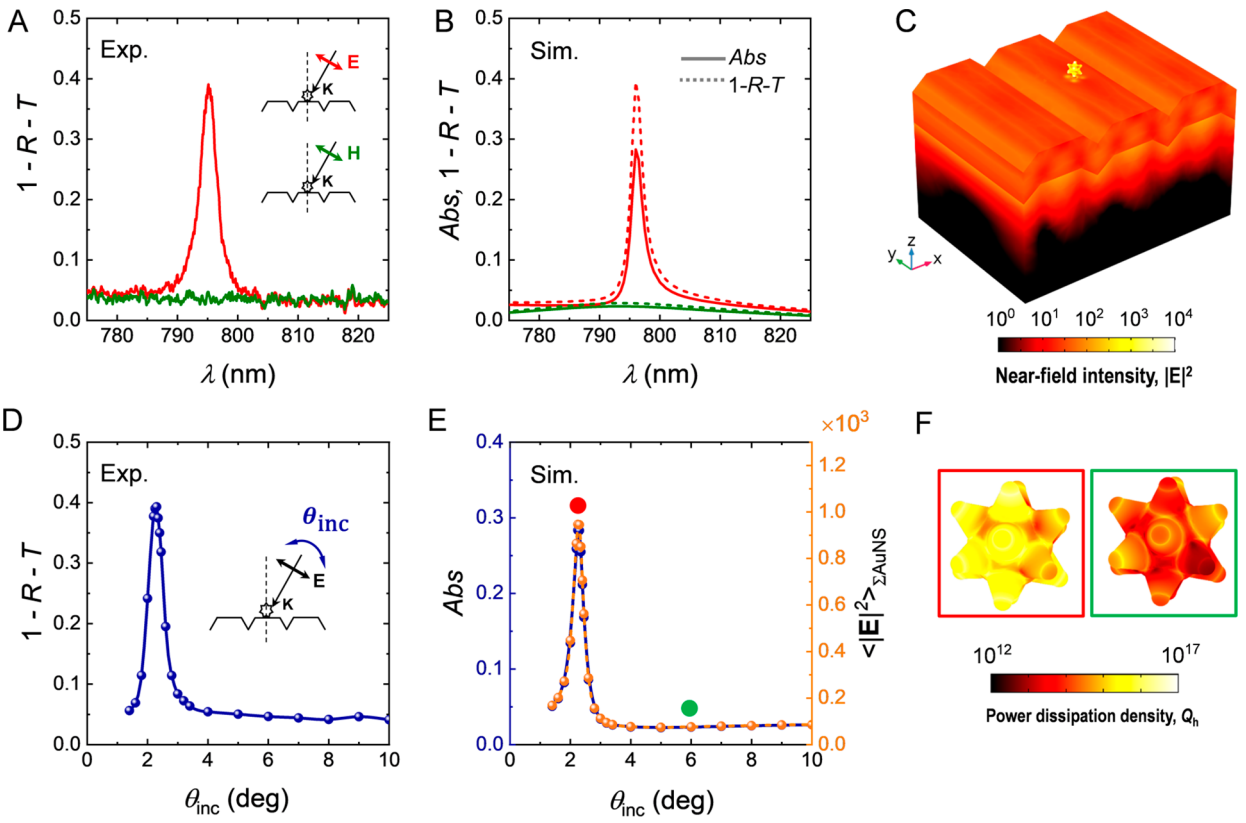

Figure 2. PCGR-mediated AuNS absorption enhancement. (A) Experimental 1-*R*-*T* spectra of the hybrid system at θ_{inc} = 2.3° for TM- (red) and TE- (green) polarized incident light (as indicated in the inset). (B) Simulated 1-*R*-*T* (solid line) and absorption *Abs* spectra (dashed line) of the hybrid system, under TM- (red) and TE- (green) polarized illumination. (C) Normalized near-field intensity $|\mathbf{E}|^2$ profile of the hybrid resonance at [TM, θ_{inc} = 2.3°, λ = 795 nm] (TiO_2 coated on the AuNS not shown). (D) Measured evaluation of 1-*R*-*T* at [TM, λ = 795 nm] as a function of θ_{inc} (as indicated in the inset). (E) Simulated *Abs* (navy) and normalized average electric field intensity on the AuNS surface $\langle|\mathbf{E}|^2\rangle_{\Sigma AuNS}$ (orange) at [TM,λ = 795 nm] as a function of θ_{inc}. (F) Power dissipation density (unit W/m^3) profile of the AuNS at different illumination conditions as indicated in (E). Incident field intensity: 1 MW/m^2.

absorption and scattering solely from far-field measurements, our numerical simulation reveals that absorption dominates the extinction 1-*R*-*T* (Figure 2B), directly associating 1-*R*-*T* enhancement with absorption amplification. We demonstrate that compared to solitary AuNSs, the PCGR-coupled ones produce a large and narrowband absorption enhancement that is tunable across a broad spectral range (Figure 1D).

For clarity, we first focus on one PCGR mode, which is brought to on-resonance with the AuNSs ($\lambda_{PCGR} = \lambda_{AuNS}$ = 795 nm) at incidence angle θ_{inc} = 2.3°. The far-field properties of the hybrid system were measured under both polarizations, and the resulting 1-*R*-*T* spectra at θ_{inc} = 2.3° are shown in Figure 2A. Upon activation of the cavity mode under TM polarization (red), superimposed on a broad-band extinction background, a pronounced Lorentzian-line-shaped sharp peak appears, whose spectral location is dictated by the PCGR. In contrast, the absence of a cavity mode under transverse electric (TE) polarization (green) corresponds to an extinction overlapping the background in the TM-polarized case. The background is associated with the solitary antenna modes without cavity coupling, while the sharp peak manifests the cavity-empowered antenna resonances. At first glance, it is tempting to interpret it as signatures of electromagnetically induced absorption (EIA).[34] However, the occurrence of absorption enhancement here does not involve any manipulation of the retardation phase shift,[35] or specific configurations of coupling and loss rates,[36,37] which are often necessary to enter the EIA regime.

Furthermore, we performed angle-resolved far-field measurements of the hybrid under TM polarization. Figure 2D depicts the evolution of its optical response at λ = 795 nm, as the incidence angle θ_{inc} is scanned approaching and departing from the resonance angle. Derived from the phase matching condition of the PCGR mode, the hybrid resonance also presents strong angle dependence, further validating the cavity's role in absorption amplification. The 10× enhancement of extinction 1-*R*-*T* mediated by an on-resonant cavity is in stark contrast to the abrupt suppression of absorption observed in plasmonic nanoantenna−WGM couplings, where the antenna is rendered transparent by an on-resonant cavity.[19,20,23] Given the AuNSs surface density of approximately 0.7 μm^{-2} here, the apparent extinction cross section of a PCGR-coupled AuNS is σ_{ext} = 0.4/0.7 μm^{-2} = 0.57 μm^2, which is 1 order of magnitude higher than that of a solitary AuNS, and much larger than its physical dimension. The large effective cross section illustrates the antenna's ability to capture and interact with light, and is a result of the synergistic combination of an extended photon lifetime and a strong mode confinement.[38]

A near-field optical picture is required to understand the underlying physics of the far-field spectral features of the hybrid resonance. We performed finite element method simulation (COMSOL Multiphysics) of the hybrid structure

DOI: 10.1021/acs.nanolett.9b01764
Nano Lett. XXXX, XXX, XXX−XXX

as sketched in Figure 1A. The simulated optical properties of the AuNS−PCGR hybrid (Figure 2B and 2E) show good agreement with the experiments. Importantly, Figure 2B shows that the absorption directly calculated from power dissipation in the AuNS dominates the total extinction 1-*R*-*T*. Figure 2E depicts that the incidence angle dependent absorption and the average near-field intensity on the AuNS surface (normalized to the incident field) $\langle |\mathbf{E}|^2 \rangle_{\Sigma AuNS} = \int_{\Sigma AuNS} |\mathbf{E}|^2 dr^2 / \int_{\Sigma AuNS} dr^2$ share identical evolution trend, which is as expected since the transition rate for absorption of a photon is proportional to the electric field intensity.[29] In other words, an enhancement of the nanoantenna's absorption is tantamount to an elevation of the local field intensity at the nanoantenna.

In comparison to solitary nanoantennas, the cavity-coupled ones can effectively trap light and induce a large near-field enhancement. The simulated normalized electric field intensity $|\mathbf{E}|^2$ profile of the hybrid resonance at [TM,θ_{inc} = 2.3°, λ = 795 nm] is shown in Figure 2C, where the standing-wave pattern in the corrugated TiO_2 film originates from interference between two counterpropagating PCGRs, and the very large field intensity localized at the AuNSs signifies the antennas' role in nanometer-scale focusing and boosting of optical energy. Again, the symbiotic relationship between the antenna and cavity modes departs from Fano interferences, indicating that a different modal interaction mechanism is responsible for cooperative enhancement. Figure 2F compares the dissipation power density in the AuNS when the PCGR is on-resonance (θ_{inc} = 2.3°, red box) and off-resonance (θ_{inc} = 6°, green box) as indicated in Figure 2E. It is noteworthy that, in contrast to several reported perfect absorbers where dissipation is distributed over an extended surface area,[39,40] here strong absorption is realized using a few nanoparticles, offering intriguing opportunities to empower light−matter interactions at the single nanoparticle level.[41] In addition, hybridization preserves the multiple intrinsic hotspots at the AuNS tips, ideal for enhancing plasmonic hot carrier gernation and extraction, which depend fundamentally on optical absorption and have preference for regions that combine high curvature with high near-field intensity.[42]

In essence, the delocalized PCGR mode serves as a conduit of energy from the far field to the near field, accumulating strong optical energy to feed the antennas. The PCGRs dominate the antennas in interaction with the external radiation through phase matching across its large surface area. As the PCGR effectively captures the excitation field and circulates the photons within the cavity, it produces an intense optical field that significantly modifies the photonic environment of the antenna. A much stronger near-field excitation of the antenna leads to prominent enhancement of its local field intensity and absorption. The profound reduction of resonance line width for cavity-coupled antennas is induced by effective "dilution" of plasmonic dissipation with a large lossless dielectric cavity; that is, photons recycling through the cavity effectively prolong the lifetime of the hybrid mode.

Our plasmonic−photonic hybrid enjoys unprecedented spectral tunability. The measured transmittance spectra of the hybrid system (Figure 3A colormap) as a function of incidence angle exhibits a band diagram reminiscent of that of the PCGRs. The resonance spectral location can be correctly described using phase matching conditions $\beta_{\pm} = \frac{2\pi}{\lambda}\sin(\theta_{inc}) \pm \frac{2\pi}{P}$ (Figure 3A white dashed lines), where $\beta_{\pm}$ are the propagation constants of counterpropagating TM_0

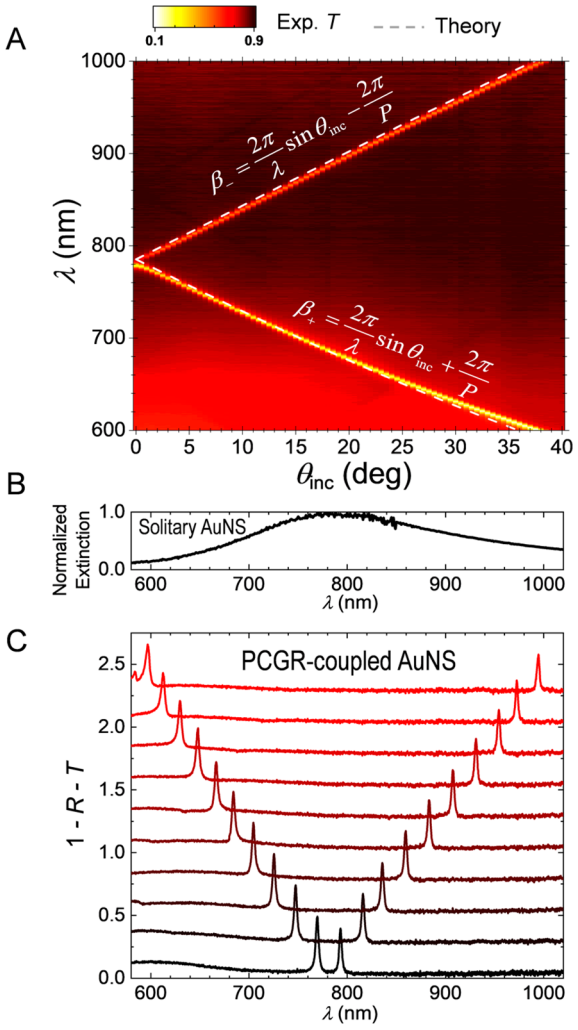

Figure 3. Spectrally tunable plasmonic−photonic hybrid resonance. (A) Experimentally measured transmittance spectrum of the hybrid resonator as a function of θ_{inc} (colormap). Band diagram of the TM_0 PCGR predicted analytically from phase-matching conditions is overlaid (white dashed curves). (B) Experimentally measured extinction spectrum of solitary AuNSs without cavity coupling. (C) Measured 1-*R*-*T* spectra of the hybrid system at various incident angles from θ_{inc} = 2° (bottom trace) to θ_{inc} = 38° (top trace) in interval of 4°. The traces are consecutively offset by 0.25.

guided modes in the air/TiO_2/SiO_2 dielectric slab waveguide, and *P* represents the lattice constant of the PC slab. The broad-band nature of the plasmon resonance of solitary AuNSs (Figure 3B) gives rise to wide spectral tunability of the hybrid mode. Figure 3C depicts the evolution of 1-*R*-*T* spectra of the hybrid system as θ_{inc} is increased from 2° to 38°. Interestingly, large absorption amplification is retained and continuously tunable across the 600−1000 nm wavelength range, even though the absorption of solitary antennas is weak at extended spectral ranges. The conservation of the Lorentzian line shape is remarkable.[19,23] In comparison, the absorption line shapes of a gold nanoparticle coupled to a WGM are sculpted by their frequency detuning: when $\omega_a = \omega_c$, the Fano interference is always destructive; when $\omega_a > \omega_c$, the Fano interference is constructive at lower freqency but destructive at higher frequency; when $\omega_a < \omega_c$, the asymmetry is reversed and the interference is constructive at higher frequency but destructive at lower frequency. The spectrally tunable absorption enhance-

DOI: 10.1021/acs.nanolett.9b01764
Nano Lett. XXXX, XXX, XXX−XXX

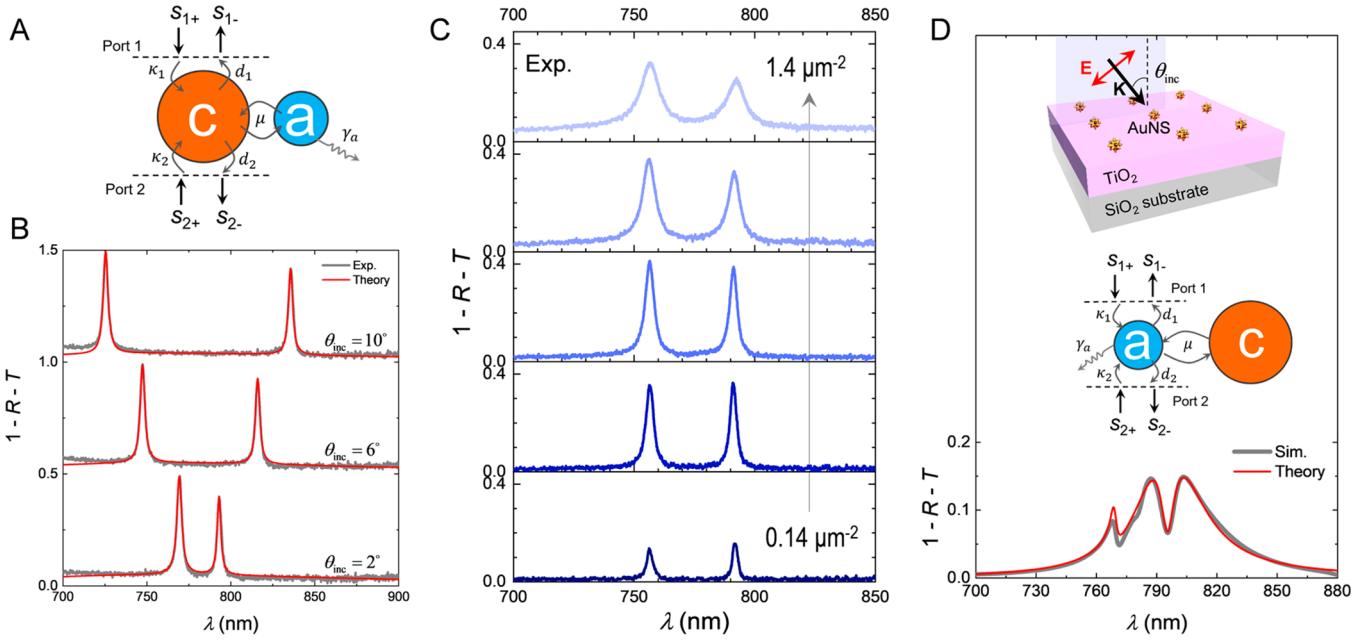

Figure 4. Key to cooperative antenna−cavity coupling. (A) TCMT model describing the AuNS−PCGR coupling. A generalized cavity mode (amplitude c) couples to an antenna mode (amplitude a and damping rate γ_a) with coupling strength μ. The cavity exchanges energy with the incoming $s_{(1,2)+}$ and outgoing $s_{(1,2)-}$ waves associated with the two ports with coupling rates $\kappa_{(1,2)}$ and $d_{(1,2)}$, respectively. (B) Extinction spectra of a hybrid structure at θ_{inc} = 2°, 6°, and 10°; the experiments (gray) and TCMT fitting (red) are overlaid. Traces are consecutively offset by 0.5. (C) (From bottom to top panel) 1-R-T spectra of hybrid composites with increasing AuNS surface density at θ_{inc} = 3°. The density ranges from 0.14 to 1.4 μm^{-2}. (D) Overlay of simulated (gray) and TCMT fitted (red) extinction spectra of the AuNS-array-on-waveguide hybrid structure (top inset), at [TM,θ_{inc} = 2.3°]. Lower inset: TCMT model describing the Fano optical pathways of the array-on-waveguide structure.

ment of the PCGR-coupled nanoparticle makes it ideally suitable for applications like on-chip photodetectors and spectrometers.[43] In addition, this hybridization concept can be readily extended to the mid-infrared range, promising ultrasensitive surface enhanced infrared absorption spectroscopy, where the strong, ultrasharp hybrid resonances can be spectrally tuned through angle multiplexing to match the molecular vibrational fingerprints.[44]

The antenna−PCGR interaction can be accounted by TCMT,[45] as schematically depicted in Figure 4A. The cavity resonance (mode amplitude c, central frequency ω_c, and damping rate γ_c) communicates with the external radiation and at the same time couples to an antenna mode (amplitude a, central frequency ω_a, damping rate γ_a). We first decouple the antenna mode from the external radiation on the assumption that its near-field interaction with the cavity is significantly stronger than with direct far-field radiation. The corresponding dynamic coupled mode equations read

$$\frac{\mathrm{d}}{\mathrm{d}t}\begin{pmatrix} c \\ a \end{pmatrix} = \left[j\begin{pmatrix} \omega_c & \mu \\ \mu & \omega_a \end{pmatrix} - \begin{pmatrix} \gamma_c & 0 \\ 0 & \gamma_a \end{pmatrix} \right] \begin{pmatrix} c \\ a \end{pmatrix} + \sqrt{\frac{A_c}{A_i}} \begin{pmatrix} \kappa_1 & \kappa_2 \\ 0 & 0 \end{pmatrix} \begin{pmatrix} s_{1+} \\ s_{2+} \end{pmatrix} \tag{1}$$

$$\begin{pmatrix} s_{1-} \\ s_{2-} \end{pmatrix} = C\begin{pmatrix} s_{1+} \\ s_{2+} \end{pmatrix} + c\begin{pmatrix} d_1 \\ d_2 \end{pmatrix} \tag{2}$$

where s_{1+}, s_{1-}, and s_{2-} are the incoming, reflected, and transmitted waves respectively (s_{2+} = 0); A_c and A_i are the effective aperture of the cavity, and area of excitation beam, respectively; μ is the intermodal coupling strength; $\kappa_{1,2}$ and $d_{1,2}$ are the coupling with incoming and outgoing waves, respectively; and scattering matrix C describes a direct transport process.

Consider a mirror symmetric system we obtain the cavity-mediated extinction as

$$1\text{-}R\text{-}T = \frac{2\gamma_c\gamma_\mu}{(\omega - (\omega_c + \omega_\mu))^2 + (\gamma_c + \gamma_\mu)^2}\frac{A_c}{A_i} \tag{3}$$

where $\omega_\mu = \frac{\mu^2(\omega-\omega_a)}{(\omega-\omega_a)^2+\gamma_a^2}$ and $\gamma_\mu = \frac{\mu^2\gamma_a}{(\omega-\omega_a)^2+\gamma_a^2}$. Equation 3 represents a narrowband absorption peak in the vicinity of the cavity mode, and its Lorentzian line shape is maintained regardless of resonance frequency detuning. The frequency shift and line width broadening of the hybrid eigenmode induced by nanoparticle coupling predicted by TCMT match exactly with the well-known Bethe−Schwinger cavity perturbation theory.[46] The broadband background can be described by the extinction of solitary antennas. Figure 4B shows the extinction spectra of a hybrid at different θ_{inc}, exhibiting good agreement between our experiments (gray) and analytical model (red) (the slightly higher experimental background when λ < 720 nm corresponds to the onset of Rayleigh anomaly in the quartz substrate). Here the intermodal coupling strength μ is the only free parameter in the fitting, while all other parameters are extracted from experiments or simulations (Supporting Information).

Figure 4C exhibits the extinction spectra of hybrid composites with increasing AuNS surface densities (0.14−1.4/μm^2). A higher density of AuNSs corresponds to a larger extinction background. Meanwhile, this versatile platform offers widely tunable resonance line widths while maintaining enhancements. Interestingly, as the density rises, the 1-R-T peaks first increase and then decrease, contrary to conventional

DOI: 10.1021/acs.nanolett.9b01764
Nano Lett. XXXX, XXX, XXX−XXX

wisdom that more nanoparticles induce higher absorption. Intuitively, the cavity can be understood as a matching network for the antenna,[47] as it manipulates the antenna's radiative damping through mediating the external radiation, and suppresses the antenna's absorptive damping through mode hybridization. Larger AuNS density maps to larger total plasmonic−photonic coupling μ and results in a larger absorptive damping rate and thus broader resonance line widths (TCMT fitting shown in Figure S10). The maximum power transferred to the antenna is obtained via critical coupling (or conjugate matching), that is, matching the radiative damping (associated with PCGR Q-factor) to the absorptive damping (associated with AuNS density). Experiments show a maximum extinction value of 0.4 (Figure 4C middle panel, density $\sim$0.7 μm^{-2}), which can be improved further by employing a reflector under the cavity.[48] An important inference follows that, by using a high-Q cavity, the maximum absorption will be achieved with very few nanoparticles, so that each nanoantenna delivers a very large absorption cross section, enabling ultrastrong light−matter interaction at its hotspots.

The distinct optical excitation pathway is a vital ingredient for the realization of cooperative plasmonic−photonic coupling. Opposite to the Fano interference underlying both EIT and EIA where cavity resonance is the dark mode providing a backaction onto the bright antenna resonance, here the narrowband cavity acts as the "bright" resonance that communicates with the external radiation and mediates the activation of the "dark" broad-band antenna resonance. It is insightful to compare our result with an antenna-array-on-waveguide structure where the AuNSs are periodically arranged on the surface of an air/TiO_2/SiO_2 slab waveguide (Figure 4D top inset). This system also supports hybridization of the plasmonic resonance with the PCGR mode, however with a different flow of light: light scattered from collective oscillation of the antenna array subsequently activates the PCGR in the underneath waveguide (Figure 4D bottom inset). To allow direct comparisons, we designed the structure to have the same resonance frequencies as those of the AuNS−PC slab hybrid. Figure 4D depicts the overlay of the simulated (gray) and TCMT predicted (red) 1-R-T spectrum of this structure at [TM, θ_{inc} = 2.3°]. The Fano interaction model correctly describes its hybridization: superimposed on the broadband antenna resonance, a sharp dip occurs when the cavity and antenna are on-resonance, and an asymmetric spectral feature appears when they are detuned. The result is in line with experimental observations of a very similar structure.[49] Therefore, we show that similar building blocks (AuNS and PCGR) can lead to drastically different coupling scenarios depending on the order of mode excitation, and an optical pathway enabling cavity-mediated excitation of an antenna is indispensable for a cooperative interaction.

In summary, we unambiguously demonstrated strong, spectrally tunable absorption enhancement in the AuNSs mediated by a PCGR cavity mode. Our experiments, numerical simulations, and theoretical model provide a comprehensive picture of the combination of a cavity's Q-factor and an antenna's mode confinement. We elucidated the physics underlying the cooperative plasmonic−photonic hybridization, which includes an optical pathway highlighting the cavity-mediated excitation of the antenna and a balance between the cavity's Q-factor and the antennas' density. These findings can be generalized to inspire the synergistic integration of different types of cavities and antennas. Complementary to the Fano interference framework, we opened up a new avenue to sculpting enhanced light−matter interactions with on-demand line widths, spectral detuning, and enhancement factors, which would benefit a broad scope of applications and technologies.

■ ASSOCIATED CONTENT

Supporting Information

The Supporting Information is available free of charge on the ACS Publications website at DOI: 10.1021/acs.nanolett.9b01764.

Materials and methods (sample fabrication and characterization, spectroscopic measurements); numerical simulations; modeling the antenna−cavity hybrid system; effect of AuNS density; further discussions on optical pathways; optical properties of the bare PC slab; tuning the plasmonic resonance of the solitary AuNSs; effect of nanoantennas' location on PC slab (PDF)

■ AUTHOR INFORMATION

Corresponding Author

*E-mail: bcunning@illinois.edu.

ORCID

Qinglan Huang: 0000-0001-8337-1947

Notes

The authors declare no competing financial interest.

■ ACKNOWLEDGMENTS

This work is supported by the National Science Foundation (Grant 1512043). Q.H. thanks the Sah Fellowship at the University of Illinois, Urbana−Champaign. The authors are grateful to Dr. Jui-Nung Liu for his participation in the design and implementation of instrument used to gather 1-R-T data and useful discussions. Dr. Liu declined to be listed as a coauthor for this paper. The authors would like to acknowledge Dr. Kathy Walsh and Dr. Jade Wang at the Materials Research Laboratory for assistance in material characterization.

■ REFERENCES

(1) Agio, M.; Alù, A. *Optical antennas*; Cambridge University Press: 2013.

(2) Aslam, U.; Rao, V. G.; Chavez, S.; Linic, S. *Nat. Catal* **2018**, *1* (9), 656−665.

(3) Baffou, G.; Quidant, R. *Laser Photonics Rev.* **2013**, *7* (2), 171−187.

(4) Kinkhabwala, A.; Yu, Z. F.; Fan, S. H.; Avlasevich, Y.; Mullen, K.; Moerner, W. E. *Nat. Photonics* **2009**, *3* (11), 654−657.

(5) Nie, S.; Emory, S. R. *Science* **1997**, *275* (5303), 1102−6.

(6) Neubrech, F.; Huck, C.; Weber, K.; Pucci, A.; Giessen, H. *Chem. Rev.* **2017**, *117* (7), 5110−5145.

(7) Zhou, W.; Dridi, M.; Suh, J. Y.; Kim, C. H.; Co, D. T.; Wasielewski, M. R.; Schatz, G. C.; Odom, T. W. *Nat. Nanotechnol.* **2013**, *8* (7), 506−11.

(8) Kauranen, M.; Zayats, A. V. *Nat. Photonics* **2012**, *6* (11), 737−748.

(9) Tame, M. S.; McEnery, K. R.; Ozdemir, S. K.; Lee, J.; Maier, S. A.; Kim, M. S. *Nat. Phys.* **2013**, *9* (6), 329−340.

(10) Maier, S. A. Localized Surface Plasmons. In *Plasmonics: Fundamentals and Applications*; Maier, S. A., Ed.; Springer US: New York, NY, 2007; pp 65−88.

(11) Sonnichsen, C.; Franzl, T.; Wilk, T.; von Plessen, G.; Feldmann, J.; Wilson, O.; Mulvaney, P. *Phys. Rev. Lett.* **2002**, *88* (7), 077402.

DOI: 10.1021/acs.nanolett.9b01764
Nano Lett. XXXX, XXX, XXX−XXX

(12) Chanda, D.; Shigeta, K.; Truong, T.; Lui, E.; Mihi, A.; Schulmerich, M.; Braun, P. V.; Bhargava, R.; Rogers, J. A. *Nat. Commun.* **2011**, *2*, 479.
(13) Schmidt, M. A.; Lei, D. Y.; Wondraczek, L.; Nazabal, V.; Maier, S. A. *Nat. Commun.* **2012**, *3*, 1108.
(14) Xiao, Y. F.; Liu, Y. C.; Li, B. B.; Chen, Y. L.; Li, Y.; Gong, Q. H. *Phys. Rev. A: At., Mol., Opt. Phys.* **2012**, *85* (3), 031805.
(15) Barth, M.; Schietinger, S.; Fischer, S.; Becker, J.; Nusse, N.; Aichele, T.; Lochel, B.; Sonnichsen, C.; Benson, O. *Nano Lett.* **2010**, *10* (3), 891−5.
(16) Saleh, B. E.; Teich, M. C.; Saleh, B. E. *Fundamentals of photonics*; Wiley: New York, 1991; Vol. *22*.
(17) Liu, J.-N.; Huang, Q.; Liu, K.-K.; Singamaneni, S.; Cunningham, B. T. *Nano Lett.* **2017**, *17* (12), 7569−7577.
(18) Peng, B.; Ozdemir, S. K.; Chen, W.; Nori, F.; Yang, L. *Nat. Commun.* **2014**, *5*, 5082.
(19) Heylman, K. D.; Thakkar, N.; Horak, E. H.; Quillin, S. C.; Cherqui, C.; Knapper, K. A.; Masiello, D. J.; Goldsmith, R. H. *Nat. Photonics* **2016**, *10* (12), 788.
(20) Ruesink, F.; Doeleman, H. M.; Verhagen, E.; Koenderink, A. F. *Phys. Rev. Lett.* **2018**, *120* (20), DOI: 10.1103/PhysRevLett.120.206101.
(21) Peng, P.; Liu, Y. C.; Xu, D.; Cao, Q. T.; Lu, G.; Gong, Q.; Xiao, Y. F. *Phys. Rev. Lett.* **2017**, *119* (23), 233901.
(22) Doeleman, H. M.; Verhagen, E.; Koenderink, A. F. *ACS Photonics* **2016**, *3* (10), 1943−1951.
(23) Thakkar, N.; Rea, M. T.; Smith, K. C.; Heylman, K. D.; Quillin, S. C.; Knapper, K. A.; Horak, E. H.; Masiello, D. J.; Goldsmith, R. H. *Nano Lett.* **2017**, *17* (11), 6927−6934.
(24) Gurlek, B.; Sandoghdar, V.; Martín-Cano, D. J. A. P. *ACS Photonics* **2018**, *5* (2), 456−461.
(25) Rodriguez, S. R. K.; Abass, A.; Maes, B.; Janssen, O. T. A.; Vecchi, G.; Rivas, J. G. *Phys. Rev. X* **2011**, *1* (2), 021019.
(26) Haus, H. A. *Waves and fields in optoelectronics*; Prentice-Hall: 1984.
(27) Fan, S.; Suh, W.; Joannopoulos, J. D. *J. Opt. Soc. Am. A* **2003**, *20* (3), 569−72.
(28) Fan, S. H.; Joannopoulos, J. D. *Phys. Rev. B: Condens. Matter Mater. Phys.* **2002**, *65* (23), 235112.
(29) Chuang, S. L. *Physics of photonic devices*; John Wiley & Sons: 2012; Vol. *80*.
(30) Novotny, L.; van Hulst, N. *Nat. Photonics* **2011**, *5* (2), 83−90.
(31) Kong, X. T.; Wang, Z. M.; Govorov, A. O. *Adv. Opt. Mater.* **2017**, *5* (15), DOI: 10.1002/adom.201600594.
(32) Mayer, K. M.; Hafner, J. H. *Chem. Rev.* **2011**, *111* (6), 3828−57.
(33) Vecchi, G.; Giannini, V.; Rivas, J. G. *Phys. Rev. B: Condens. Matter Mater. Phys.* **2009**, *80* (20), DOI: 10.1103/PhysRevB.80.201401.
(34) Floess, D.; Hentschel, M.; Weiss, T.; Habermeier, H.-U.; Jiao, J.; Tikhodeev, S. G.; Giessen, H. *Phys. Rev. X* **2017**, *7* (2), 021048.
(35) Taubert, R.; Hentschel, M.; Kastel, J.; Giessen, H. *Nano Lett.* **2012**, *12* (3), 1367−71.
(36) Tassin, P.; Zhang, L.; Zhao, R.; Jain, A.; Koschny, T.; Soukoulis, C. M. *Phys. Rev. Lett.* **2012**, *109* (18), 187401.
(37) Adato, R.; Artar, A.; Erramilli, S.; Altug, H. *Nano Lett.* **2013**, *13* (6), 2584−91.
(38) Zhou, W.; Odom, T. W. *Nat. Nanotechnol.* **2011**, *6* (7), 423−7.
(39) Mauser, K. W.; Kim, S.; Mitrovic, S.; Fleischman, D.; Pala, R.; Schwab, K. C.; Atwater, H. A. *Nat. Nanotechnol.* **2017**, *12* (8), 770−775.
(40) Li, W.; Valentine, J. *Nano Lett.* **2014**, *14* (6), 3510−4.
(41) Brongersma, M. L.; Halas, N. J.; Nordlander, P. *Nat. Nanotechnol.* **2015**, *10* (1), 25−34.
(42) Cortes, E.; Xie, W.; Cambiasso, J.; Jermyn, A. S.; Sundararaman, R.; Narang, P.; Schlucker, S.; Maier, S. A. *Nat. Commun.* **2017**, *8*, DOI: 10.1038/ncomms14880.
(43) Sobhani, A.; Knight, M. W.; Wang, Y.; Zheng, B.; King, N. S.; Brown, L. V.; Fang, Z.; Nordlander, P.; Halas, N. J. *Nat. Commun.* **2013**, *4*, 1643.
(44) Tittl, A.; Leitis, A.; Liu, M.; Yesilkoy, F.; Choi, D. Y.; Neshev, D. N.; Kivshar, Y. S.; Altug, H. *Science* **2018**, *360* (6393), 1105−1109.
(45) Adato, R.; Altug, H. *Nat. Commun.* **2013**, *4*, 2154.
(46) Waldron, R. *Proc. Inst. Electr. Eng., Part C* **1960**, *107* (12), 272−274.
(47) Doeleman, H. *Hybrid resonators for light trapping and emission control*; Universiteit van Amsterdam: 2019.
(48) Piper, J. R.; Fan, S. *ACS Photonics* **2014**, *1* (4), 347−353.
(49) Linden, S.; Kuhl, J.; Giessen, H. *Phys. Rev. Lett.* **2001**, *86* (20), 4688−4691.

DOI: 10.1021/acs.nanolett.9b01764
Nano Lett. XXXX, XXX, XXX−XXX